IEEE Access
Multidisciplinary ⋮ Rapid Review ⋮ Open Access Journal

Received 22 November 2022, accepted 23 December 2022, date of publication 27 December 2022,
date of current version 5 January 2023.

Digital Object Identifier 10.1109/ACCESS.2022.3232726

RESEARCH ARTICLE

Simulation of Dynamic Resistance and Total Loss of HTS CORC Cables

YUKAI QIAO, YUEMING SUN, RODNEY A. BADCOCK, (Senior Member, IEEE), NICHOLAS M. STRICKLAND, AND ZHENAN JIANG, (Senior Member, IEEE)
Robinson Research Institute, Victoria University of Wellington, Wellington 6012, New Zealand

Corresponding author: Zhenan Jiang (zhenan.jiang@vuw.ac.nz)

This work was supported in part by the China Scholarship Council (CSC); in part by the New Zealand Ministry of Business, Innovation and Employment, under Contract RTVU1707; and in part by the Strategic Science Investment Fund Advanced Energy Technology Platforms under Contract RTVU2004.

ABSTRACT In some high temperature superconducting (HTS) applications, HTS coated conductors carry DC current under external AC magnetic fields. Dynamic resistance occurs when the amplitude of the magnetic field is greater than the threshold magnetic field of the coated conductors. The resulting AC loss, termed as total loss, consists of dynamic loss due to dynamic resistance and magnetization loss due to the shielding currents caused by the AC magnetic field. Conductor on round core (CORC) cables wound with HTS coated conductors have attracted broad attention due to their large current-carrying capability and mechanical flexibility for coil applications. However, there has been no report on dynamic resistance and total loss in CORC cables. In this work, we present 3D FEM simulation results on the dynamic resistance and total loss of a spiral tape and three CORC cables, based on the $\boldsymbol{T}-\boldsymbol{A}$ formulation. The number of layers of the CORC cables, the amplitude of the AC magnetic field and transport DC current levels have been varied to study the impact of those parameters on dynamic resistance and total loss of the three CORC cables. The simulation results show that magnetization loss without current in a spiral tape can be analytically estimated by Brandt and Indenbom's theoretical equation for a superconducting strip under perpendicular AC magnetic field with a geometric coefficient $2/\pi$. Furthermore, dynamic resistance of the spiral tape and each tape in a single-layer cable can be predicted by the analytical equation for a strip carrying DC current under perpendicular AC magnetic field, also taking into account the geometric coefficient $2/\pi$. The simulation results also show that the difference of total loss values in the three CORC cables depends on the shielding effect: the more layers of CORC cables, the lower each loss component. The two-layer Cable with each tape in the outer layer sitting on top of the tape in the inner layer has the lowest loss and the highest threshold magnetic field.

INDEX TERMS AC loss, CORC cables, dynamic resistance, high temperature superconductors, 3D modeling, $\boldsymbol{T}-\boldsymbol{A}$ formulation.

I. INTRODUCTION

Rare-Earth Barium Copper Oxide (REBCO) high-temperature superconducting (HTS) coated conductors become promising candidates for power applications, such as rotating machines [1], [2], [3], flux pumps [4], [5] and persistent current switches [6], [7], [8], due to their excellent in-field critical current performance. In those HTS devices, HTS coated conductors are exposed to an AC magnetic field while carrying a DC current. Once the applied magnetic field exceeds the threshold magnetic field, a non-zero DC resistance occurs in the superconductors and this effect is known as dynamic resistance [9], [10], [11], [12]. Two types of losses are generated under this condition: one is magnetization loss due to shielding currents caused by the external magnetic field; the other is dynamic loss from dynamic resistance due to the interaction of the DC current and AC magnetic field. The sum of the two loss components, termed as total loss,

The associate editor coordinating the review of this manuscript and approving it for publication was Guillaume Parent.

leads to a parasitic heat load and influences the efficiency of the cooling system of the HTS devices.

To date, many previous works on dynamic resistance and total loss have mainly focused on single HTS coated conductor tapes [12], [13], [14], [15], [16], [17] or stacks [3], [18], [19], [20], [21], [22], [23]. In terms of the operating conditions, the dependence of dynamic resistance and total loss of single REBCO coated conductors on magnetic field/DC current/temperature/frequency have been investigated through experiments [13], [14], [15]. Dynamic resistance and total loss of a three-tape HTS stack have been measured where both magnetization loss and dynamic loss in the stack were smaller than a single tape due to the shielding effect [18]. Simulations based on 2D $\boldsymbol{H}$-formulation have studied the dynamic resistance/loss and total loss of single REBCO coated conductors and stacks [16], [17], [21]. In addition, the derived analytical equations developed for dynamic resistance of single REBCO coated conductors or stacks carrying DC currents under perpendicular magnetic fields had good agreement with both finite-element model (FEM) simulation and experimental results [17], [23].

The Conductor on Round Core (CORC) cables offer high current-carrying capacity and mechanical strength, hence are becoming one of the most practical HTS conductors for high-field magnets, compact superconducting power cables and field windings of rotating machines [24], [25], [26]. Many previous works have measured either magnetization loss under AC magnetic field without current or transport loss carrying AC current without the external applied field [27], [28], [29], [30], [31]. Regarding numerical modellings, the 3D models based on $\boldsymbol{H}$ formulation or $\boldsymbol{T}-\boldsymbol{A}$ formulation have been carried out to validate the experimental results [27], [32], [33], [34]. However, there has been no report on dynamic resistance and total loss on CORC cables up to now, even though they are critical to the applications mentioned in the above.

To address the research gap, this paper presents 3D FEM simulation results of a spiral tape and three CORC cables (see Fig. 1) assembled with 4mm-wide REBCO coated conductors. The temperature is assumed fixed at 77 K, the self-field DC critical current of the REBCO tape is set at 100 A. The FEM simulations are based on $\boldsymbol{T}-\boldsymbol{A}$ formulation and implemented in COMSOL 5.6 [35]. The geometrical and physical properties of the spiral tape and the three CORC cables are from [27], and the associated parameters are listed in Table 1. Magnetization loss, dynamic resistance/loss, and total loss in the spiral tape and CORC cables are simulated. The reduced DC current $i = I_{dc}/I_c$, the ratio of transport DC current to the self-field critical current, ranges from 0.3 to 0.9, and the amplitude of the external AC magnetic fields is up to 100 mT. The current density distribution normalized by critical current density, J/J_c, and magnetic field lines of the spiral tape and CORC cables are compared to understand the obtained AC loss characteristics.

II. NUMERICAL MODELLING

A. T-A FORMULATION

3D FEM models were built to simulate the magnetization loss, dynamic resistance/loss, and total loss in the spiral tape and three CORC cables, as shown in Fig. 1, based on $\boldsymbol{T}-\boldsymbol{A}$ formulation [35], [36], [37] using COMSOL 5.6. To reduce the computation time, only one full twist pitch length of the four models is considered based on their periodic structures.

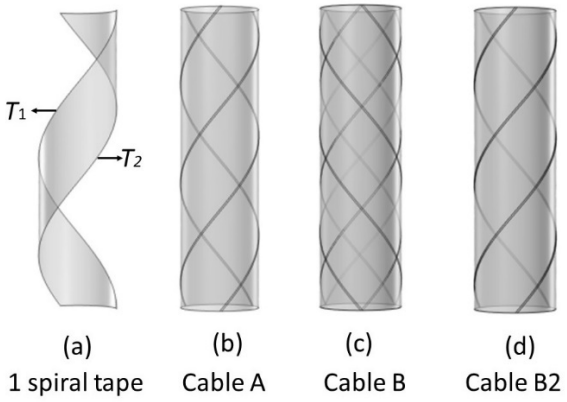

FIGURE 1. Schematics of four models: A spiral tape, one-layer Cable A, two-layer Cable B with opposite winding direction and two-layer Cable B2 with same winding direction (fully overlapping tapes).

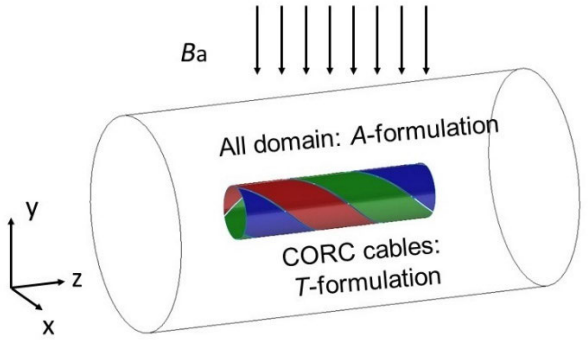

FIGURE 2. FEM model of $T-A$ formulation using T formulation only for CORC cable and A formulation for the whole domain, with DC current transporting along the spiral tape and exposed to AC magnetic field in the y-direction.

TABLE 1. Key parameters of CORC cables.

Parameters	Spiral tape	Cable A	Cable B/B2
No. of layers	/	1	2
No. of tapes per layer	/	3	6
O.D of layer (mm)	/	5.14	5.14/5.28
Winding angle	40°	40°	40°
Width of tape (mm)	4	4	4
Pitch (mm)	19	19	19
Winding direction	/	/	Opposite/same

In the simulations, the spiral tape and three CORC cables transport DC currents under an AC magnetic field, which are

surrounded by an air domain. Fig. 2 gives the schematic of the modelling for Cable A. For the four studied models, the current vector potential $\boldsymbol{T}$ is applied to the superconductors and the magnetic vector potential $\boldsymbol{A}$ is imposed to the whole domain.

$\boldsymbol{J}$ in the superconductors is defined as the curl of the current vector potential $\boldsymbol{T}$ as shown in Eq. (1). $\boldsymbol{T}$ is always perpendicular to conductor surface [35], [36], [37], [38].

$$\boldsymbol{J} = \nabla \times \boldsymbol{T} = \begin{bmatrix} \frac{\partial T_z}{\partial y} - \frac{\partial T_y}{\partial z} \\ \frac{\partial T_x}{\partial z} - \frac{\partial T_z}{\partial x} \\ \frac{\partial T_y}{\partial x} - \frac{\partial T_x}{\partial y} \end{bmatrix} \tag{1}$$

where T_{x}, T_{y} and T_{z} are the x, y and z components of $\boldsymbol{T}$ in the Cartesian coordinates.

According to Faraday's law (Eq. (2)) and $\boldsymbol{E}-\boldsymbol{J}$ power law (Eq. (3)), the $\boldsymbol{T}$-based equation governing equation is derived as Eq. (4).

$$\nabla \times \boldsymbol{E} = -\frac{\partial \boldsymbol{B}}{\partial t} \tag{2}$$

$$\boldsymbol{E} = E_c \left(\frac{\boldsymbol{J}}{J_c(B)}\right)^{n-1} \left(\frac{\boldsymbol{J}}{J_c(B)}\right) = \rho \boldsymbol{J} \tag{3}$$

$$\nabla \times (\rho \nabla \times \boldsymbol{T}) = -\frac{\partial \boldsymbol{B}}{\partial t} \tag{4}$$

where $\boldsymbol{E}$ and $\boldsymbol{B}$ are the electrical field and magnetic flux density. E_{c} =1 μV/cm is the characteristic electrical field and n =31 is the exponent of $E-J$ curve. ρ represents the resistivity of superconductors. $J_{\mathrm{c}}(\boldsymbol{B})$ is the magnetic field-dependent critical current density of superconductors, given by Eq. (5).

$$J_c(\boldsymbol{B}) = \frac{J_c 0}{(1 + \frac{\sqrt{(kB_{para}^2 + B_{per}^2)}}{B_0})^a} \tag{5}$$

where B_{para} and B_{per} are the parallel and perpendicular magnetic field components, respectively. $k = 0.0605$, $\alpha = 0.7580$, $B_0 = 103$ mT are three fitting parameters from the previous work [27].

According to Ampere's law, the $\boldsymbol{A}$-based governing equation is given by Eq. (6).

$$\nabla \times \nabla \times \boldsymbol{A} = \mu_0 \boldsymbol{J} \tag{6}$$

To calculate dynamic resistance and total loss, the numerical simulation was set as a two-step study. The DC current, I_{dc}, is first injected to the spiral tape or the CORC cable via a ramp function, I_{r}(t), and Dirichlet boundary condition is used for I_{r}(t), as given in Eq. (7).

$$I_{dc} = I_r(t) = Rt = \oint \boldsymbol{T} \cdot d\boldsymbol{l} = (T_2 - T_1) \cdot \delta \tag{7}$$

where $R = 1000$ A/s is a constant ramping rate and t is the ramping time to a given DC current value. T_1 and T_2 are the values of $\boldsymbol{T}$ at both longitudinal edges of the spiral tape, as shown in Fig. 1(a). $\delta = 1$ μm is the thickness of the superconducting layer.

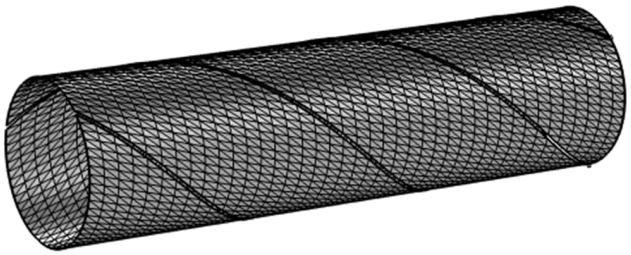

FIGURE 3. Mesh configuration of CORC cable with 20 elements along the lateral direction and 40 elements along longitudinal direction.

TABLE 2. Loss magnitudes and computation time on three mesh densities.

Mesh	DOF	Time	Q_{m} (J/Hz)	Q_{dyn} (J/Hz)
20+40	28215	10min20s	1.1613e-2	1.4353e-3
30+60	52449	1h48min	1.1530e-2	1.4479e-3
40+80	85615	4h28min	1.1485e-2	1.4559e-3

The DC current is then held constant while an AC magnetic field, $B_{\mathrm{a}} = B_{\mathrm{m}}\sin(2\pi ft)$ with magnitude B_{m} and frequency f, is applied onto the air domain in the y-direction via a Dirichlet boundary condition, given by Eq. (8). The total loss, Q_{total}, can be calculated by Eq. (9), and comprises dynamic loss Q_{dyn} given by Eq. (10) and magnetization loss (Q_{m}):

$$B = (0, B_a, 0) \tag{8}$$

$$Q_{total} = \int_0^{\frac{1}{f}} \delta dt = \int \boldsymbol{E} \cdot \boldsymbol{J} dS = Q_m + Q_{dyn} \tag{9}$$

$$Q_{dyn} = \int_0^{\frac{1}{f}} E_{ave} I_{dc} dt \tag{10}$$

$$E_{ave} = \frac{\int \boldsymbol{E}(t) \cdot dS}{S} \tag{11}$$

where S is the surface of the superconductor, and E_{ave} is the average magnetic field along the tape surface, given by Eq. (11). A frequency of 130 Hz was used in this simulation.

B. THE INFLUENCE OF MESH DENSITY

A mapped mesh is applied to the superconductor and free tetrahedra to the air domain. To improve the computing efficiency, three different mapped mesh densities were tested for the spiral tape: 20 + 40; 30 + 60; 40 + 80, where the first number is the element number across the lateral direction of the tape and the second one is the element number along the longitudinal direction. Then the mapped mesh is converted to triangular elements by inserting diagonal edges. Taking the spiral tape as an example, two loss components were calculated at $B_{\mathrm{m}} = 50$ mT and $i = 0.3$. The loss values and computation time using the three different mesh densities are compared in Table. 2. The difference of Q_{m} and Q_{dyn} values between the 20+40 and 40+80 is approximately 1.4% and 1.1%, respectively. However, the computation time for 40+80 is 28 times more than that of 20+40. If scaling up the spiral tape to the CORC cables using 40+80, the computation

for the CORC cables takes several days only to improve the accuracy by 2%. Thus, mesh density of 20+40 is selected for each spiral tape of CORC cables in this work as shown in Fig. 3.

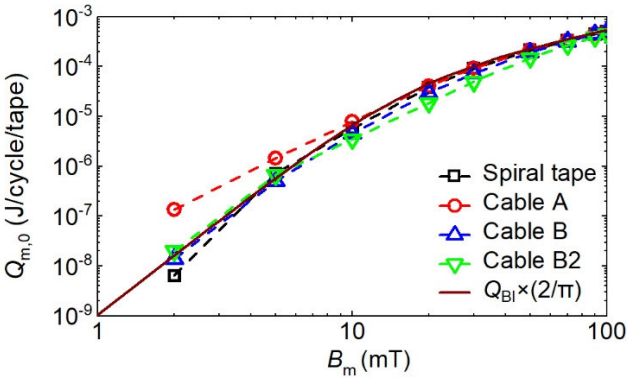

FIGURE 4. Magnetization loss per tape of four samples without current, $Q_{m,0}$, as a function of the magnetic field amplitude up to 100 mT. The analytical equation with geometric coefficient, $Q_{BI}\times(2/\pi)$, is also plotted.

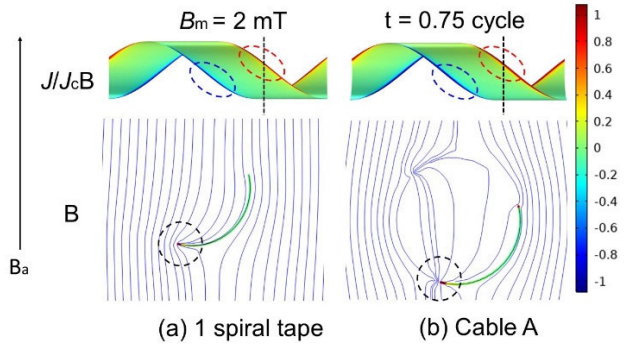

FIGURE 5. Normalized current density, $J/J_c(B)$, and magnetic field line distributions of the spiral tape and the equivalent tape of Cable A under 2 mT at $t = 0.75$ cycle with no transport current.

III. SIMULATION RESULTS AND DISCUSSION

A. MAGNETIZATION LOSS

1) ZERO DC CURRENT

Fig. 4 shows the simulated magnetization loss without DC current, $Q_{m,0}$, for the four configurations versus the amplitude of the AC magnetic fields up to 100 mT. The loss is shown per cycle and per tape. The analytical magnetization loss from Brandt and Indenbom equation for a single superconducting strip under an AC perpendicular magnetic field, Q_{BI}, multiplied by a geometric coefficient $2/\pi$ (effective width for a spiral tape compared with a straight tape), is also plotted in Fig. 4 and the length of the strip used in the equation is the real length of the spiral tape [39].

Fig. 4 shows that the simulated $Q_{m,0}$ of the spiral tape has a good agreement with $Q_{BI}\times(2/\pi)$ except the value at 2 mT. Furthermore, $Q_{m,0}$ per tape in Cable A below 10 mT is larger than that in the spiral tape. These differences are explained

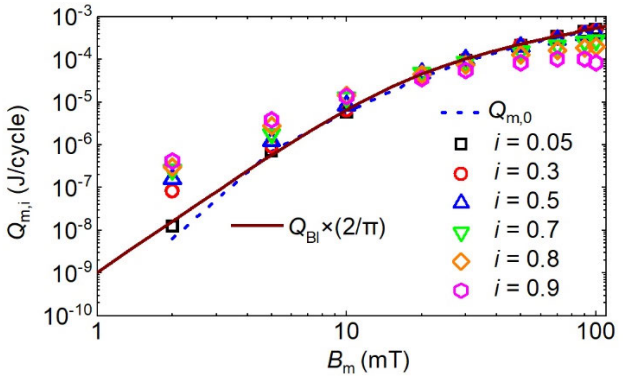

FIGURE 6. Magnetization loss with DC current, $Q_{m,i}$, of the spiral tape at six reduced DC current levels.

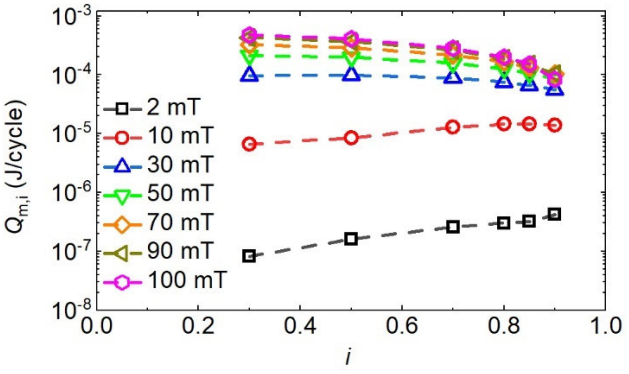

FIGURE 7. Magnetization loss of the spiral tape with DC current, $Q_{m,i}$, versus reduced current i at magnetic field amplitudes ranging from 2 mT to 100 mT.

by Fig. 5, where the normalized current density distributions, J/J_c, and magnetic field lines around the cross-section (cut across the black dashed lines) of the spiral tape are compared with the equivalent tape in Cable A when $B_m = 2$ mT. At $t = 0.75$ cycle, the shielding current regions, highlighted with the red and blues circles, of Cable A are noticeably wider than those of the spiral tape, where the superconducting tape is fully penetrated ($J/J_c > 1$) and magnetization loss is generated. As shown in the the figure, the edges of the spiral tape in Cable A are exposed to more perpendicular magnetic field than that of the spiral tape, due to the superposition of the magnetic fields generated from the neighboring tapes in Cable A. The larger penetrated regions account for the higher $Q_{m,0}$ values of Cable A at low magnetic field amplitudes. In addition, there exists clear difference in Fig. 4 that $Q_{m,0}$ of two-layer Cables B and B2 are smaller than that of a spiral tape and Cable A at low and medium magnetic field amplitudes. This phenomenon stems from the shielding effect in Cable B and B2 due to their multi-layer structure, and similar results have been observed in [27]. The difference in $Q_{m,0}$ values between Cable B, B2 and the spiral tape, Cable A becomes smaller with increasing the amplitude of the magnetic field and ultimately disappears when $B_m > 90$ mT. This is due to the nature of shielding effect that weakens with

increasing the magnetic field and completely disappear once the amplitude of the external magnetic field is much greater than the effective penetration field [14], [18].

2) NON-ZERO DC CURRENT

Fig. 6 compares the simulated magnetization loss, $Q_{\mathrm{m,i}}$, of the spiral tape as a function of the amplitude of the magnetic field for six DC current levels. $Q_{\mathrm{m},0}$ of the spiral tape and the analytical equation $Q_{\mathrm{BI}}\times(2/\pi)$ are also plotted. At $i = 0.05$, $Q_{\mathrm{m,i}}$ values nearly overlap with $Q_{\mathrm{m},0}$ values. When $B_{\mathrm{m}} < 10$ mT, the simulated $Q_{\mathrm{m,i}}$ values are one to two order magnitude higher than $Q_{\mathrm{m},0}$ for $0.3 \leq i \leq 0.9$, whilst $Q_{\mathrm{m,i}}$ values become smaller than $Q_{\mathrm{m},0}$ at high-B when $i > 0.5$. The behaviors have been observed in previous studies for a single REBCO tape or a three-tape REBCO stack [14], [16]. At low current and low field, the current-carrying capacity of HTS tape is large enough to accommodate both the DC current and the shielding current, and $Q_{\mathrm{m,i}}$ is determined by the amplitude of external magnetic field and DC current nearly has no influence on $Q_{\mathrm{m,i}}$. For high current and high field, the region for shielding currents shrinks, and this in turn causes the reduced $Q_{\mathrm{m,i}}$ values.

To further analyze the magnetization loss values of the spiral tape, $Q_{\mathrm{m,i}}$ values under different magnetic field amplitudes (up to 100 mT) are replotted versus the reduced DC current i ($0.3 \leq i \leq 0.9$) in Fig. 7. At 2 mT, $Q_{\mathrm{m,i}}$ grows monotonically with increasing i; $Q_{\mathrm{m,i}}$ reaches maximum at $i = 0.9$ for 10 mT; $Q_{\mathrm{m,i}}$ values decrease monotonically once $B_{\mathrm{m}} \geq 30$ mT. Similar tendency also has been observed in a three-tape HTS stack where the magnetization loss $Q_{\mathrm{m,i}}$ behaviors have been explained via remanent magnetization which was determined by the asymmetric internal current distribution (consists of the DC current and the induced shielding currents) in the superconductors [18].

B. DYNAMIC RESISTANCE

The dynamic resistance, R_{dyn}, of a superconducting strip per unit length per cycle has been analytically obtained through Eq. (12) [13].

$$\frac{R_{dyn}}{fL} = \frac{4a}{I_{c0}}(B_a - B_{th}) \tag{12}$$

where a is the half-width of the superconducting strip, B_{a} is the amplitude of the applied magnetic field and B_{th} is a threshold field for the onset of dynamic resistance. The B_{th} values have been experimentally shown to agree well with Eq. (13) in the case of $i > 0.2$ and Eq. (14) for $i \leq 0.2$ [14], [15], [16], [17], [18].

$$B_{th1} = \frac{4.9284\mu_0 J_{c0} d}{2\pi}(1 - i) \tag{13}$$

$$B_{th2} = \frac{\mu_0 J_{c0} d}{4\pi}\left(\frac{1}{i} ln\left(\frac{1+i}{1-i}\right) + \ln\left(\frac{1-i^2}{4i^2}\right)\right) \tag{14}$$

where d is the half-thickness of the strip. Considering the shape of the spiral tape, geometric coefficient $2/\pi$ should be considered into Eq. (12) to obtain the R_{dyn} for the spiral tape, i. e. Eq. (15) should be used for the R_{dyn} of the spiral tape.

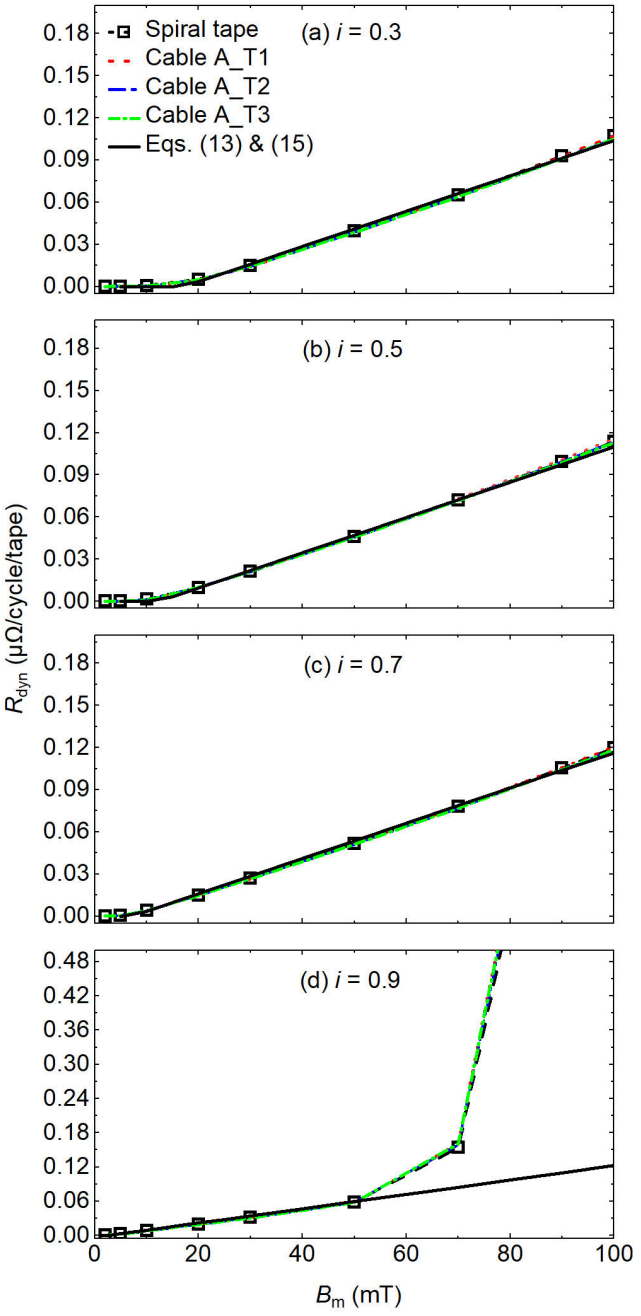

FIGURE 8. Dynamic resistance comparison between the spiral tape and each tape of Cable A at four different DC current levels. The analytical results from the combined Eqs. (13) and (15) are also plotted.

Fig.8 compares the simulated R_{dyn} values of the spiral tape

$$\frac{R_{dyn}}{fL} = \frac{2}{\pi} \times \frac{4a}{I_{c0}}(B_a - B_{th}) \tag{15}$$

and each tape of Cable A, plotted as a function of the external magnetic field amplitude for four different i values. R_{dyn} values obtained from combined Eqs. (13) and (15) for a spiral tape are also plotted. Fig. 8 shows that analytical R_{dyn}

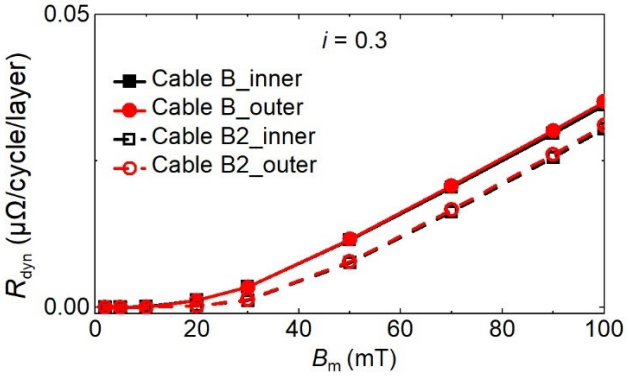

FIGURE 9. Dynamic resistance comparison between each layer in Cable B and Cable B2 at $i = 0.3$.

values from the combined Eqs. (13) and (15) have a good agreement with the simulated results of each tape at each i. For any given DC current, there is no difference of R_{dyn} values between each tape in the Cable A and R_{dyn} values of the spiral tape. When $i = 0.9$, a non-linear flux-flow resistance occurs at high-B in the spiral tape [16]. This is because the field-dependent critical current of a HTS tape falls below the transporting DC current.

Fig. 9 presents the simulated R_{dyn} values per layer for Cable B and Cable B2 versus the external magnetic field amplitude at $i = 0.3$. In both Cable B and Cable B2, R_{dyn} values of the inner layer agree well with the values of the outer layer. The same results are observed for the other DC current levels. Fig.10 shows the R_{dyn} values per layer for Cable A, B and B2 plotted as a function of the external magnetic field amplitude when $0.3 \leq i \leq 0.9$. Only R_{dyn} values from the inner layer of Cable B and Cable B2 are presented based on the layer-independent result in Fig. 9. R_{dyn} values of the one-layer Cable A remain the highest at each i; the two-layer Cable B2 with the same winding direction for the tapes in the inner and outer layers has the strongest shielding effect (shielding effect is maximized in this case because the inner and outer layers are perfectly aligned), hence has the lowest R_{dyn} values for $i = 0.3$ and $i = 0.5$. With increasing i, the simulated R_{dyn} values of Cable B and Cable B2 almost overlap due to diminishing shielding effect.

Fig. 11 compares the simulated B_{th} values per tape of the spiral tape and three CORC cables. The analytically obtained B_{th} values from Eq. (13) are plotted as well. The simulated B_{th} values shown here are obtained by fitting the linear section of the R_{dyn} curves which intercept the x-axis. Since there is no difference in dynamic resistance values between the spiral tape and each tape in Cable A, as shown in Fig. 8, the B_{th} values of the spiral tape and Cable A per tape overlap at any DC current levels. The curve from analytical Eq. (13) is also close to the simulated results for the spiral tape and Cable A. For the two-layer CORC cables, Cable B2 has greater shielding effect than Cable B, leading to the largest B_{th} values at low-i. With the increasing i, the difference between two-layer CORC cables becomes smaller due to the weakened shielding effect.

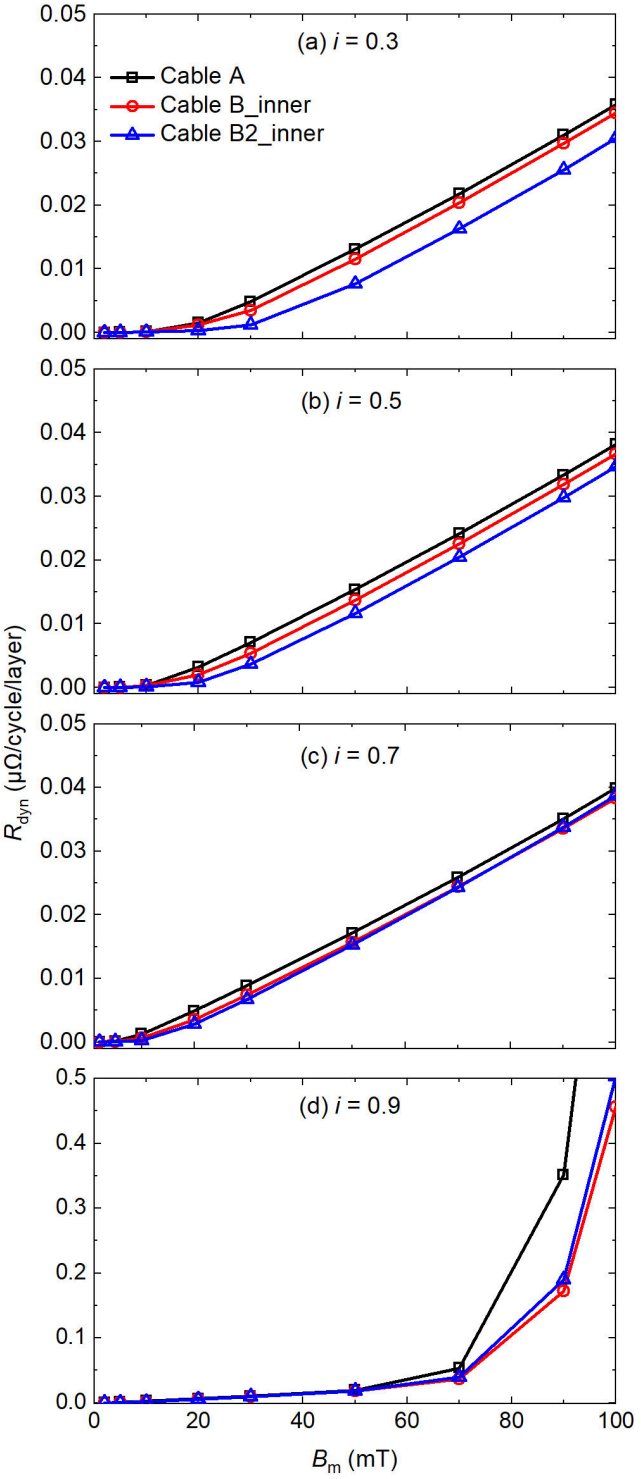

FIGURE 10. Dynamic resistance comparison between the inner layers of Cable A, Cable B and Cable B2 at four DC current levels.

To better distinguish the magnetization loss from dynamic resistance/loss, Fig. 12 shows the normalized current density distribution, and only the green spiral tape of Cable A in

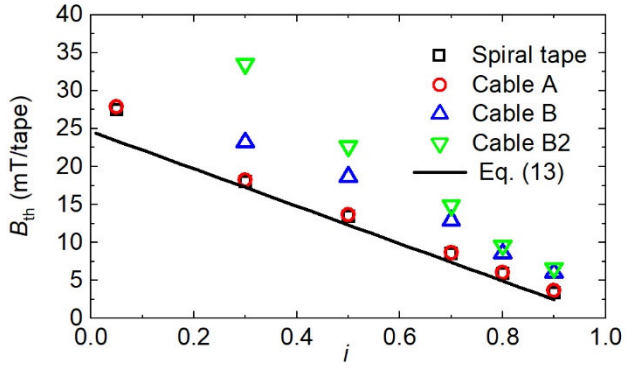

FIGURE 11. Threshold magnetic field comparison between four samples. Eq. (13) for a superconducting stirp is also plotted.

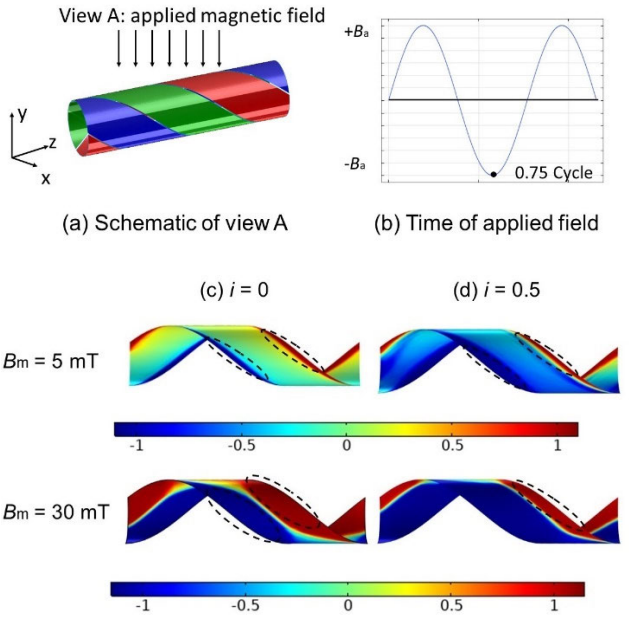

FIGURE 12. Normalized current density distribution of the green spiral tape of Cable A with or without DC current injection when $B_a = 5$ mT and $B_a = 30$ mT respectively at $t = 0.75$ cycle.

Fig. 12(a) is presented for simplicity. The distributions are shown for the negative peak of the applied field, as shown in Fig. 12(b). When $B_a = 5$ mT and $B_a = 30$ mT for $i = 0$ (Fig. 12(c)) and $i = 0.5$ (Fig. 12(d)). when $i = 0$, from view A, it clearly shows only shielding currents are induced at the edges, as highlighted in black circles where magnetization loss is generated. No current flows in the central region, which is consistent to previous papers [14], [15], [16], [17], [18]. When $i = 0.5$ and $B_a = 5$ mT, there is no dynamic resistance as shown in Fig. 8(b). This is because the central region of the tape is fully shielded and does not experience any applied field and DC current flows in the central region of the spiral tape, with J/J_c approximately equal to 0.5. Magnetization loss is generated at the edges of the spiral tape, as highlighted in the black circles. In contrast, when $B_a = 30$ mT, the amplitude of the external magnetic field is larger than

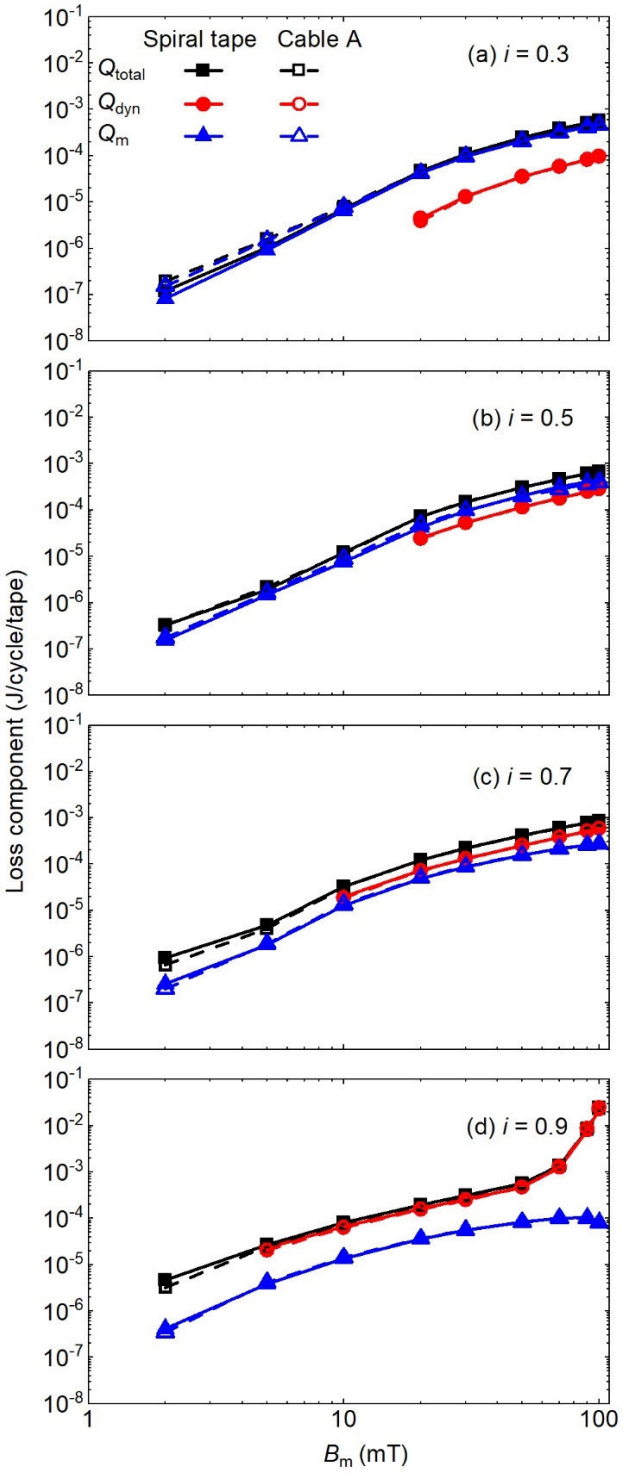

FIGURE 13. Total loss Q_{total} and loss components, $Q_{m,i}$ and Q_{dyn}, for the spiral tape and Cable A as a function of the magnetic field amplitude at four DC current levels.

the threshold magnetic field B_{th} (13. 85 mT from Fig. 11), the central region is no longer shielded such that $|J/J_c(B)| > 1$, except for a very thin current-reversal region [22]. In this case, a net flow of magnetic flux traverses the DC current-flowing region, leading to the occurrence of dynamic resistance/loss.

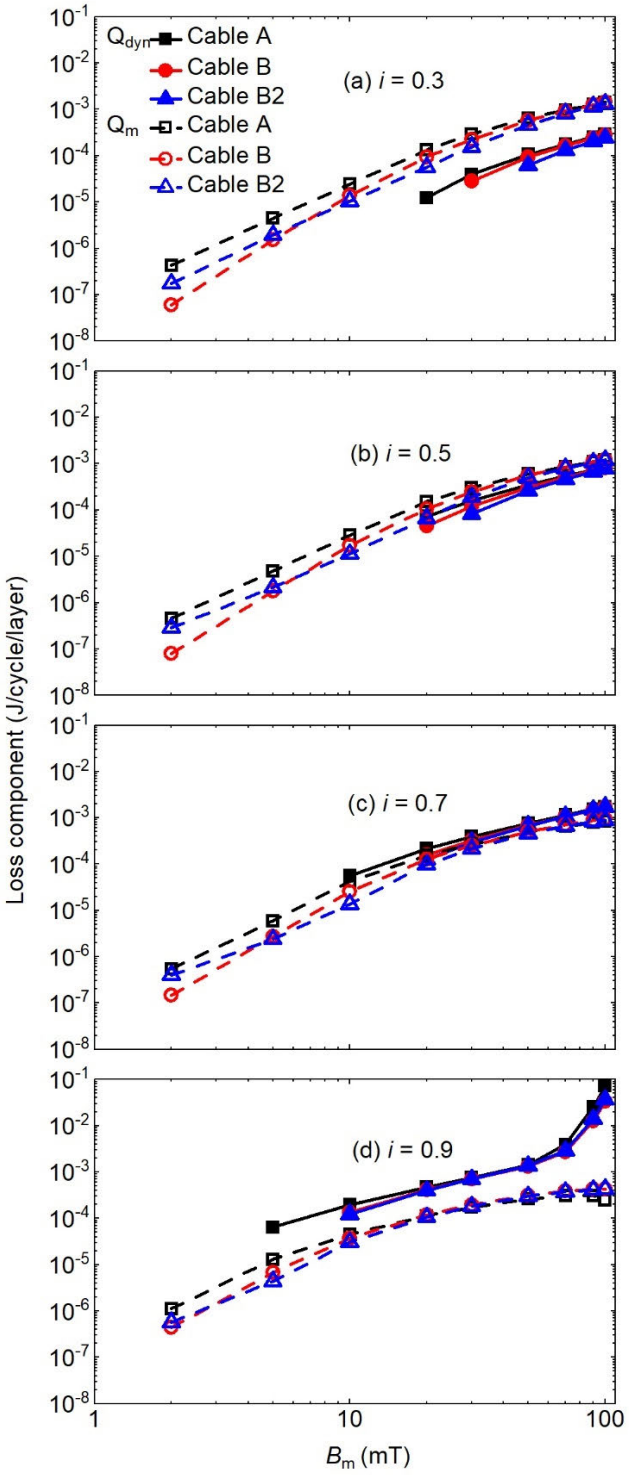

FIGURE 14. Loss components $Q_{m,i}$ and Q_{dyn} of each layer in Cable A, Cable B and Cable B2 as a function of magnetic field at four DC current levels.

C. TOTAL LOSS AND LOSS COMPONENT

The simulated total loss (Q_{total}) and its components ($Q_{m,i}$ and Q_{dyn}) per tape between the spiral tape and Cable A are plotted in Fig. 13, as a function of the magnetic field amplitudes up to 100 mT when $0.3 \leq i \leq 0.9$. Q_{dyn} values below threshold

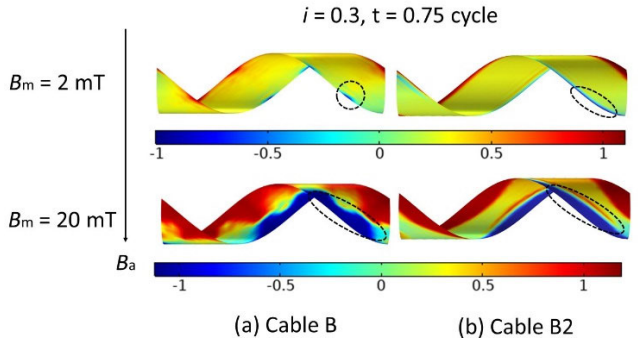

FIGURE 15. Normalized current density distribution of inner layer of Cable B and Cable B2 under two different magnetic field amplitudes while $i = 0.3$, at $t = 0.75$ cycle.

magnetic field are omitted in the plot. The loss components per tape of the spiral tape and Cable A are very similar. From Fig. 13(a)-(d), the contribution of each loss component to the total loss varies with the DC current level. $Q_{m,i}$ plays a dominant role in Q_{total} throughout the magnetic field range compared with Q_{dyn} when $i = 0.3$ and nearly one order larger than Q_{dyn} at 100 mT, as shown in Fig. 13(a). When i increases to 0.5, the dominance of $Q_{m,i}$ weakens, and Q_{dyn} becomes slightly lower than $Q_{m,i}$ as can be seen in Fig. 13(b). However, Q_{dyn} is greater than $Q_{m,i}$ when $i = 0.7$, as shown in Fig. 13(c). At $i = 0.9$, Q_{dyn} nearly overlaps with Q_{total} (see Fig. 13 (d)) due to the dominance of the flux-flow loss, and similar loss behaviors have been observed in single REBCO tapes and a three-tape REBCO stack [14], [15], [18].

Fig. 14 compares the two simulated loss components, $Q_{m,i}$ and Q_{dyn}, per layer of Cable A, Cable B and B2, plotted as a function of the magnetic field amplitude at four different i values. In this figure, we also omit the Q_{dyn} values below the B_{th} values. For each CORC cable, $Q_{m,i}$ values are approximately one order higher than Q_{dyn} at $i = 0.3$, as shown in Fig. 14(a). At $i = 0.5$ and 0.7, the difference of the two loss components becomes smaller, and Q_{dyn} ultimately exceeds $Q_{m,i}$ at $i = 0.9$ as can be seen from Fig. 14(d). This is due to the occurrence of flux-flow loss. Among the three CORC cables, both loss components of Cable A remain the highest at any current level, and those of Cable B2 are the lowest for $B_m > 5$ mT due to it having the strongest shielding effect.

To investigate the result at 2 mT, Fig. 15 shows the J/J_c distribution of a tape in the inner layer of Cable B and Cable B2 at $i = 0.3$ at 2 mT and 20 mT, respectively. At $t = 0.75$ cycle, wider shielding current regions at the edges are observed in Cable B2 at 2 mT compared with that of Cable B, as highlighted using the black circles where magnetization loss is generated. This should be due to the difference of winding direction of Cables B and B2, where the two layers of Cable B2 are perfectly aligned and applied magnetic field can freely penetrate at the edges between tapes, while the interwoven cable structure of Cable B only allows the magnetic field penetration from the small resultant gaps. As a result, $Q_{m,i}$ value of Cable B2 is greater than that of Cable B at 2 mT.

When $B_a = 20$ mT, shielding current regions of Cable B2 are smaller than Cable B due to stronger shielding effect of Cable B2 than that of B leading to a lower $Q_{m,i}$ value. Thus, a crossover of $Q_{m,i}$ values appears at the low and medium magnetic field amplitudes for Cable B and B2, as presented in Fig. 14.

IV. CONCLUSION

In this work, 3D models based on *T-A* formulation have been built to simulate magnetization loss, dynamic resistance/loss, and total loss of a spiral tape and three CORC cables which are assembled from 4 mm-wide REBCO coated conductors. The normalized DC current i ranges from 0.005 to 0.9 and the amplitude of the magnetic fields is up to 100 mT.

$Q_{m,0}$ of the spiral tape can be analytically estimated using the analytical equation $Q_{BI}\times(2/\pi)$, where $2/\pi$ is the geometric coefficient. $Q_{m,i}$ of the spiral tape are one to two orders higher than $Q_{m,0}$ when $B_m < 10$ mT for $i \leq 0.3$ and becomes smaller than $Q_{m,0}$ at high-B when $i > 0.5$. For high i and high B, the region for shielding currents shrinks, and this in turn causes the reduction in $Q_{m,i}$ values.

R_{dyn} of the spiral tape and each tape of Cable A can be analytically predicted empirically predicted by the combined Eqs. (13) and (15) which considers the geometric coefficient $2/\pi$. No difference has been observed between each layer of either Cable B or Cable B2 in terms of R_{dyn} values. Eq. (14), that gives B_{th} expression for a superconducting strip, is still effective for estimating the threshold magnetic field of the spiral tape and Cable A when $i \geq 0.3$. Because of the shielding effect from the neighboring layer for two-layer CORC cables, B_{th} values of Cable B and B2 are higher than the values for the spiral tape and each tape of Cable A. The difference of B_{th} values between the four models diminishes due to the weakened shielding effect at high i.

Total loss (Q_{total}) and the two loss components ($Q_{m,i}$ and Q_{dyn}) of the spiral tape and each tape in Cable A are indistinguishable. Among the three CORC cables, total loss of one-layer Cable A remains the highest at each i, and two-layer Cable B2 has the lowest loss due to the strongest shielding effect. At $i = 0.9$, Q_{dyn} values of all three CORC cables are higher than $Q_{m,i}$ due to the occurrence of flux-flow loss.

As far as the authors are aware, the current work is the first report on simulation results of the total loss and dynamic resistance for a spiral tape and simple CORC cables. Experiments still need to be carried out to verify these simulation results.

ACKNOWLEDGMENT

Yukai Qiao acknowledges Yue Wu for her assistance on the simulation model building. All data is provided in full in the results section of this article.

REFERENCES

[1] M. D. Ainslie, Y. Jiang, W. Xian, Z. Hong, W. Yuan, R. Pei, T. J. Flack, and T. A. Coombs, "Numerical analysis and finite element modelling of an HTS synchronous motor," *Phys. C, Supercond. Appl.*, vol. 470, no. 20, pp. 1752–1755, Nov. 2010.

[2] D. Liu, H. Polinder, N. Magnusson, J. Schellevis, and A. B. Abrahamsen, "Ripple field AC losses in 10-MW wind turbine generators with a MgB_2 superconducting field winding," *IEEE Trans. Appl. Supercond.*, vol. 26, no. 3, pp. 1–5, Apr. 2016.

[3] H. Zhang, P. Machura, K. Kails, H. Chen, and M. Mueller, "Dynamic loss and magnetization loss of HTS coated conductors, stacks, and coils for high-speed synchronous machines," *Supercond. Sci. Technol.*, vol. 33, no. 8, Aug. 2020, Art. no. 084008.

[4] Z. Jiang, K. Hamilton, N. Amemiya, R. A. Badcock, and C. W. Bumby, "Dynamic resistance of a high-Tc superconducting flux pump," *Appl. Phys. Lett.*, vol. 105, no. 11, Sep. 2014, Art. no. 112601.

[5] Z. Jiang, C. W. Bumby, R. A. Badcock, H.-J. Sung, N. J. Long, and N. Amemiya, "Impact of flux gap upon dynamic resistance of a rotating HTS flux pump," *Supercond. Sci. Technol.*, vol. 28, no. 11, Nov. 2015, Art. no. 115008.

[6] J. Geng, K. Matsuda, B. Shen, H. Zhang, X. Zhang, L. Fu, Z. Huang, and T. A. Coombs, "HTS persistent current switch controlled by AC magnetic field," *IEEE Trans. Appl. Supercond.*, vol. 26, no. 3, pp. 1–4, Apr. 2016.

[7] C. Li, J. Geng, B. Shen, X. Li, J. Gawith, J. Ma, J. Yang, and T. A. Coombs, "Persistent current switch for HTS superconducting magnets: Design, control strategy, and test results," *IEEE Trans. Appl. Supercond.*, vol. 29, no. 2, pp. 1–4, Mar. 2019.

[8] C. Li, J. Geng, J. Gawith, B. Shen, X. Zhang, H. Zhang, J. Ma, and T. A. Coombs, "Design for a persistent current switch controlled by alternating current magnetic field," *IEEE Trans. Appl. Supercond.*, vol. 28, no. 4, pp. 1–5, Jun. 2018.

[9] V. V. Andrianov, V. B. Zenkevich, V. V. Kurguzov, V. V. Sytchev, and F. F. Ternovskii, "Effective resistance of an imperfect type-II superconductor in an oscillating magnetic field," *Zhurnal Eksperimental'noi Teoreticheskoi Fiziki*, vol. 58, Aug. 1970.

[10] T. Ogasawara, Y. Takahashi, K. Kanbara, Y. Kubota, K. Yasohama, and K. Yasukochi, "Alternating field losses in superconducting wires carrying DC transport currents: Part 1 single core conductors," *Cryogenics*, vol. 19, no. 12, pp. 736–740, Dec. 1979.

[11] M. P. Oomen, J. Rieger, M. Leghissa, B. T. Haken, and H. H. J. T. Kate, "Dynamic resistance in a slab-like superconductor with $J_c(B)$ dependence," *Supercond. Sci. Technol.*, vol. 12, no. 6, pp. 382–387, Jun. 1999.

[12] H. Zhang, B. Shen, X. Chen, and Z. Jiang, "Dynamic resistance and dynamic loss in a ReBCO superconductor," *Supercond. Sci. Technol.*, vol. 35, no. 11, Nov. 2022, Art. no. 113001.

[13] M. Ciszek, O. Tsukamoto, J. Ogawa, and D. Miyagi, "Energy losses in YBCO-123 coated conductors carrying transport current in perpendicular external magnetic field," *AIP Conf. Proc.*, vol. 614, Jul. 2000, pp. 606–613.

[14] Y. Sun, J. Fang, G. Sidorov, Q. Li, R. A. Badcock, N. J. Long, and Z. Jiang, "Total loss measurement and simulation in a REBCO coated conductor carrying DC current in perpendicular AC magnetic field at various temperatures," *Supercond. Sci. Technol.*, vol. 34, no. 6, May 2021, Art. no. 065009.

[15] Y. Liu, Z. Jiang, G. Sidorov, C. W. Bumby, R. A. Badcock, and J. Fang, "Dynamic resistance measurement in a YBCO wire under perpendicular magnetic field at various operating temperatures," *J. Appl. Phys.*, vol. 126, no. 24, Dec. 2019, Art. no. 243904.

[16] M. D. Ainslie, C. W. Bumby, Z. Jiang, R. Toyomoto, and N. Amemiya, "Numerical modelling of dynamic resistance in high-temperature superconducting coated-conductor wires," *Supercond. Sci. Technol.*, vol. 31, no. 7, Jun. 2018, Art. no. 074003.

[17] Z. Jiang, R. Toyomoto, N. Amemiya, X. Zhang, and C. W. Bumby, "Dynamic resistance of a high-T_c coated conductor wire in a perpendicular magnetic field at 77 K," *Supercond. Sci. Technol.*, vol. 30, no. 3, Jan. 2017, Art. no. 03LT01.

[18] Y. Sun, J. Fang, G. Sidorov, R. A. Badcock, N. J. Long, and Z. Jiang, "Dynamic resistance and total loss in a three-tape REBCO stack carrying DC currents in perpendicular AC magnetic fields at 77 K," *Supercond. Sci. Technol.*, vol. 35, no. 3, Feb. 2022, Art. no. 035011.

[19] Y. Liu, Z. Jiang, Q. Li, C. W. Bumby, R. A. Badcock, and J. Fang, "Dynamic resistance measurement in a four-tape YBCO stack with various applied field orientation," *IEEE Trans. Appl. Supercond.*, vol. 29, no. 5, pp. 1–7, Aug. 2019.

[20] Z. Jiang, W. Zhou, C. W. Bumby, M. Staines, Q. Li, R. A. Badcock, N. J. Long, and J. Fang, "Dynamic resistance measurement of a four-tape YBCO stack in a perpendicular magnetic field," *IEEE Trans. Appl. Supercond.*, vol. 28, no. 4, pp. 1–5, Jun. 2018.

[21] J. M. Brooks, M. D. Ainslie, Z. Jiang, S. C. Wimbush, R. A. Badcock, and C. W. Bumby, "Numerical modelling of dynamic resistance in a parallel-connected stack of HTS coated-conductor tapes," *IEEE Trans. Appl. Supercond.*, vol. 30, no. 4, pp. 1–8, Jun. 2020.

[22] J. Hu, J. Ma, J. Yang, M. Tian, A. Shah, I. Patel, H. Wei, L. Hao, Y. Ozturk, B. Shen, and T. A. Coombs, "Numerical study on dynamic resistance of an HTS switch made of series-connected YBCO stacks," *IEEE Trans. Appl. Supercond.*, vol. 31, no. 5, pp. 1–6, Aug. 2021.

[23] R. Liu, W. Yang, D. Song, J. Zhu, and X. Li, "Effect of dynamic resistance on AC loss in stacked superconducting tapes," *IEEE Trans. Appl. Supercond.*, vol. 30, no. 4, pp. 1–5, Jun. 2020.

[24] D. C. van der Laan, J. D. Weiss, C. H. Kim, L. Graber, and S. Pamidi, "Development of CORC cables for helium gas cooled power transmission and fault current limiting applications," *Supercond. Sci. Technol.*, vol. 31, no. 8, Aug. 2018, Art. no. 085011.

[25] D. C. van der Laan, J. D. Weiss, and D. M. McRae, "Status of CORC cables and wires for use in high-field magnets and power systems a decade after their introduction," *Supercond. Sci. Technol.*, vol. 32, no. 3, Mar. 2019, Art. no. 033001.

[26] S. S. Kalsi, R. Badcock, J. Storey, K. A. Hamilton, and Z. Jiang, "Motors employing REBCO CORC and MgB_2 superconductors for AC stator windings," *IEEE Trans. Appl. Supercond.*, vol. 31, no. 9, pp. 1–7, Dec. 2021.

[27] Y. Wang, M. Zhang, F. Grilli, Z. Zhu, and W. Yuan, "Study of the magnetization loss of CORC cables using a 3D T-A formulation," *Supercond. Sci. Technol.*, vol. 32, no. 2, Jan. 2019, Art. no. 025003.

[28] M. Majoros, M. D. Sumption, E. W. Collings, and D. C. van der Laan, "Magnetization losses in superconducting YBCO conductor-on-round-core (CORC) cables," *Supercond. Sci. Technol.*, vol. 27, no. 12, Nov. 2014, Art. no. 125008.

[29] J. Goo, J.-W. Han, S. Lee, W.-S. Kim, K. Choi, and J.-K. Lee, "Magnetization loss of CORC with various configurations of 2G HTS strands," *IEEE Trans. Appl. Supercond.*, vol. 31, no. 5, pp. 1–5, Aug. 2021.

[30] J. Yang, C. Li, M. Tian, S. Liu, B. Shen, L. Hao, Y. Ozturk, and T. Coombs, "Analysis of AC transport loss in conductor on round core cables," *J. Supercond. Novel Magn.*, vol. 35, no. 1, pp. 57–63, Jan. 2022.

[31] J. Šouc, M. Vojenčiak, and F. Gömöry, "Experimentally determined transport and magnetization AC losses of small cable models constructed from YBCO coated conductors," *Supercond. Sci. Technol.*, vol. 23, no. 4, Apr. 2010, Art. no. 045029.

[32] J. Yang, M. Tian, J. Ma, Y. Ozturk, C. Li, J. Hu, J. Gawith, A. Shah, I. Patel, H. Wei, L. Hao, B. Shen, and T. Coombs, "Numerical study on AC loss characteristics of conductor on round core cables under transport current and magnetic field," *IEEE Trans. Appl. Supercond.*, vol. 31, no. 8, pp. 1–4, Nov. 2021.

[33] J. Sheng, M. Vojenčiak, R. Terzioglu, L. Frolek, and F. Gomory, "Numerical study on magnetization characteristics of superconducting conductor on round core cables," *IEEE Trans. Appl. Supercond.*, vol. 27, no. 4, pp. 1–5, Jun. 2017.

[34] M. Vojenčiak, A. Kario, B. Ringsdorf, R. Nast, D. C. van der Laan, J. Scheiter, A. Jung, B. Runtsch, F. Gömöry, and W. Goldacker, "Magnetization AC loss reduction in HTS CORC cables made of striated coated conductors," *Supercond. Sci. Technol.*, vol. 28, no. 10, Oct. 2015, Art. no. 104006.

[35] H. Zhang, M. Zhang, and W. Yuan, "An efficient 3D finite element method model based on the T-A formulation for superconducting coated conductors," *Supercond. Sci. Technol.*, vol. 30, no. 2, Dec. 2016, Art. no. 024005.

[36] X. Xu, Z. Huang, W. Li, X. Huang, M. Wang, Z. Hong, and Z. Jin, "3D finite element modelling on racetrack coils using the homogeneous *T-A* formulation," *Cryogenics*, vol. 119, Oct. 2021, Art. no. 103366.

[37] W. Hong, H. Liu, F. Liu, H. Jin, and S. Yi, "Improved calculation of magnetic hysteresis loss of stacked superconducting cable under T-A formulation," *IEEE Trans. Appl. Supercond.*, vol. 32, no. 6, pp. 1–5, Sep. 2022.

[38] S. You, S. S. Kalsi, M. D. Ainslie, R. A. Badcock, N. J. Long, and Z. Jiang, "Simulation of AC loss in the armature windings of a 100 kW all-HTS motor with various (RE)BCO conductor considerations," *IEEE Access*, vol. 9, pp. 130968–130980, 2021.

[39] E. H. Brandt and M. Indenbom, "Type-II-superconductor strip with current in a perpendicular magnetic field," *Phys. Rev. B, Condens. Matter*, vol. 48, no. 17, Nov. 1993, Art. no. 12893.

YUKAI QIAO received the M.E. degree in electric power and its automation from North China Electric Power University, China, in 2021. He is currently pursuing the Ph.D. degree with the Robinson Research Institute, Victoria University of Wellington, under the supervision of Zhenan Jiang and Nick Strickland. His main research interest includes the 3-D modeling of HTS materials, AC loss in stator winding of all-superconducting machines using multi-filamentary wires.

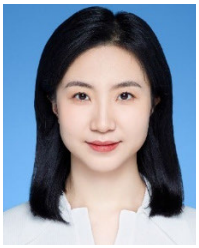

YUEMING SUN received the Ph.D. degree in electrical engineering from Beijing Jiaotong University, Beijing, China, in 2022. She is currently pursuing the second Ph.D. degree with Robinson Research Institute, Victoria University of Wellington. Her current research interests include AC loss, AC susceptibility and dynamic resistance in HTS materials, and numerical modeling for HTS devices.

RODNEY A. BADCOCK (Senior Member, IEEE) was born in Cambridge, U.K., in 1969. He received the B.Sc. degree in physics with electronics from the University of Leeds, Leeds, U.K., and the M.Sc. and Ph.D. degrees in manufacturing and materials engineering from Brunel University, U.K.

He has 30 years research experience in applied Research and Development covering manufacturing process monitoring and control, materials sensing, and superconducting systems. Since 2006, he has been concentrated on superconducting machines, production, and machines for general cable superconductors at the Robinson Research Institute, Victoria University of Wellington, Lower Hutt, New Zealand. He is currently the institute deputy director, a chief engineer, a professor and specializes in the management of complex engineering projects, including customer-focused multidisciplinary projects. He is particularly known for the development of the superconducting dynamos for electric machines and the NZ MBIE program developing aircraft superconducting electric propulsion technology. He is recognized as one of the leading experts in the application of superconducting dynamos and cables to electric machines.

Prof. Badcock was a Key Member of the Team awarded the Royal Society of New Zealand Cooper Medal, in 2008, for the development of high-temperature superconducting cables for power system applications including 1 MVA transformer, 60 MW hydro generator, and 150 MW utility generator.

NICHOLAS M. STRICKLAND received the B.Sc. (Hons.) and Ph.D. degrees in physics from the University of Canterbury, New Zealand. Since 1999, he has been with the Industrial Research Ltd., and then the Robinson Research Institute, Victoria University of Wellington, New Zealand, where he is currently a Principal Scientist. He has been involved in superconductivity research for that time, working in HTS materials, wire, and magnet development. He has a particular interest in understanding and improving flux pinning through artificial pinning centers and ion-beam irradiation of coated conductors. He is a co-developer of the SuperCurrent measurement system which reveals the critical current anisotropy of wire and tape samples over a wide parameter range of temperature and magnetic field, providing key information both for gaining a quantitative understanding of flux pinning and for magnet design. The ongoing use of this tool has led to the creation of a widely-used online database of critical current data in commercial HTS wires.

ZHENAN JIANG (Senior Member, IEEE) received the B.Eng. degree in electrical engineering from Chongqing University, Chongqing, China, in 1994, and the M.Eng. and Ph.D. degrees in applied superconductivity from Yokohama National University, Yokohama, Japan, in 2002 and 2005, respectively.

He was a Postdoctoral Research Fellow at Yokohama National University, from 2005 to 2008. He joined the Superconductivity Group currently known as the Robinson Research Institute, Victoria University of Wellington, New Zealand, in 2008, as a Research Scientist. He has a strong track record in characterization of high temperature superconductors (HTS), especially in AC loss. He is currently the principal scientist in the institute and leading an AC loss research in the institute. His recent research interests include AC loss characterization in HTS, HTS applications including transformers, flux pumps, magnets, and rotating machines.

Dr. Jiang he has been an Editorial Board Member of the journal *Superconductivity* (Elsevier), since 2021. He has been twice awarded the Japan Society for the Promotion of Science (JSPS) invitation fellowship to Kyoto University, in 2011 and 2015, respectively. He was awarded the 2021 Scott Medal from Royal Society New Zealand for his work on measuring and modeling the response of superconductors.